An extended finite element framework for vibration analysis of cracked FGM shells

Amir Nasirmanesh, Soheil Mohammadi *

High Performance Computing Lab, School of Civil Engineering, University of Tehran, Tehran, Iran

ABSTRACT

Given the widespread use of FGM shell elements in numerous industrial fields and their extreme vulnerability to crack formation, the present work is directed towards investigating the vibrational behavior of cracked FGM shells. A general XFEM formulation, with tested accuracy and performance, is presented due to its intrinsic capability to handle problems with discontinuities, such as cracks. To demonstrate the performance of the adopted approach, multiple examples are introduced and analyzed and the effects of various parameters such as the length and angle of the crack and different distribution patterns of material stiffness and density across the thickness of the shell, are extensively studied. Five cracked FGM models, including a rectangular plate, a circular plate with four radial cracks, a cylindrical shell, a conical shell and a spherical dome are simulated by the proposed approach and the results are discussed.

© 2017 Elsevier Ltd. All rights reserved.

1. Introduction

Structural shell elements comprise important parts in many engineering practices including aerospace and car industries and many others. Composite shells, which have been widely used in recent years, do not necessarily perform well in extreme conditions due to a number of defects such as delamination and debonding, especially in dynamic and cyclic loadings. To address these deficiencies, functionally graded materials (FGMs) have been developed to alleviate this phenomenon by smoothly changing the material properties across the thickness of shell.

One of the key factors that may radically influence the dynamic behavior of structures is its vibration characteristics. For example, lack of understanding and knowledge about the range of natural frequencies of the structure may lead to unforeseen phenomena such as resonance, which may risk the integrity and stability of the structure. Moreover, existence of imperfections such as dents, cracks and voids in shell structures are unavoidable and may substantially affect the overall vibrational response of the imperfect shell.

Vibration analysis of plates and shells has been the focus of researchers for many years [1–8]. Several studies have also been performed on free vibration of intact composite and FGM plates and shells. Loy et al. [9] addressed the problem of free vibration of functionally graded cylindrical shells for the first time. Based on the higher order shear deformation theory, an exact solution was obtained for a doubly-curved laminated composite shell [10] and the effects of various factors such as boundary conditions, thickness and the stacking sequence of the laminates were examined. Civalek [11] presented free vibration analysis of conical composite shells in accordance with the transverse shear deformation theory. A four variable refined theory was employed by Benachour et al. to study the free vibration of FGM plates [12]. They assessed how the gradient index of the material and the aspect ratio of the plate can affect the vibrational behavior of the FGM plate. A new application of Carrera's unified Formulation (CUF) was proposed by Neves et al. [13] for analyzing the static and free vibration of functionally graded plates. Using a high-order finite element formulation, Pradyumna and Bandyopadhyay [14] analyzed the free vibration of curved FGM panels to study the effects of rotary inertia and transverse shear. Also, the problem of vibration analysis of FGM circular plates were studied by a number of authors [15–18].

The question of how the existence of a defect such as a crack can affect the vibrational behavior of plates has drawn research attention for quite some time [19–24]. The natural frequencies of various cracked composite plates were obtained by employing the so-called Generalized Differential Quadrature Finite Element Method (GDQFEM) [25,26]. Also, the GDQFEM was successfully

used in the vibrational analysis of FGM sandwich shells with variable thicknesses [27]. A 3 D elasticity solution was presented for vibration analysis of cracked functionally graded plates by Huang et al. [28] to show how different parameters such as crack length and location can alter the natural frequency of cracked FGM plates. Recently, Joshi et al. [29] analytically investigated the effect of fiber orientation on the vibrational behavior of orthotropic plates with cracks parallel to the edges of the plate. However, no report is available on vibration analysis of cracked FGM shells.

Utilizing advanced numerical methods such as the extended finite element method (XFEM) seems logical for vibration analysis of cracked plates and shells due to the complexities brought about by the existence of cracks. The extended finite element method (XFEM) designed to improve the disadvantages of crack conformity to element edges and the refinement around the crack tips of conventional FEM for crack propagation problems [30]. The method has proved to be efficient in various discontinuity problems, as it has been successfully adopted for solving different orthotropic static [31–34], dynamic [35–37] and buckling problems [38,39]. Also, XFEM was efficiently utilized to compute the stress intensity factors of cracked composite plates [40]. Recently, Ardakani et al. [41,42] extended the method to capture the highly nonlinear stress fields around the crack tips in shape memory alloys, and the method was successfully utilized to address the thermomechanical crack propagation problem in FGM media [43–45]. In addition, there are some other techniques such as the Phantom-Node Method, the Extended Isogeometric Analysis (XIGA), and the Phase-Field Method, which have been successfully employed for analysis of cracked shells [46–49].

There are a few works that have addressed the problem of vibration analysis of cracked FGM plates by means of XFEM and XIGA [50–53]. Despite extensive studies on vibration analysis of intact FGM plates and shells, no attention has been paid to the vibrational behavior of cracked FGM shells. In this paper, for the first time, an XFEM cracked shell formulation is adopted for vibration analysis of cracked functionally graded shells. Efficiency, higher accuracy and more flexibility in dealing with various types of discontinuities with general geometries are among the main advantages of the extended finite element method compared with other numerical methods such as classical finite element method. The present method is shown to be reliable for various forms of cracked FGM shells, including cylindrical, conical and spherical shapes. Sensitivity of natural frequencies of cracked functionally graded shells are examined for various parameters such as crack length, crack angle and the distribution profile of the functionally graded material across the thickness.

The rest of the paper is organized as follows: First, the eigenvalue vibration equation for cracked FGM shells is derived using an XFEM shell discretization and presented in Section 2. Then, the present method is employed to obtain the natural frequencies and the associated mode shapes of five cracked FGM shell problems, while, thorough discussions on the obtained results are also presented. Finally, the concluding remarks on the most important obtained results are provided.

2. Formulation

In this study, a four-parameter power law distribution ($FGM_{(a/b/c/N)}$) is considered for variation of material properties, i.e. Young's modulus (E_z) and mass density (ρ_z) across the thickness of shell,

$$E_z = (E_c - E_m)\left(1 - a\left(\frac{1}{2} + \frac{Z}{h}\right) + b\left(\frac{1}{2} + \frac{Z}{h}\right)^c\right)^N + E_m \qquad (1)$$

$$\rho_z = (\rho_c - \rho_m)\left(1 - a\left(\frac{1}{2} + \frac{Z}{h}\right) + b\left(\frac{1}{2} + \frac{Z}{h}\right)^c\right)^N + \rho_m \qquad (2)$$

where the subscripts c and m denote ceramic and metal, respectively. h is the shell thickness, Z is perpendicular to the mid-surface of the shell and varies form $-h/2$ to $h/2$, as shown in Fig. 1. Also, a, b, c and N (power index) are four variables which define the material distribution profile across the thickness.

It should be mentioned that by considering $b = c = 0$, the conventional power law distribution of material is obtained, in which the bottom and top surfaces of the shell are respectively ceramic and metal, and the material properties continuously change from ceramic to metal between these two surfaces. For the proposed four-parameter power law distribution, however, the material properties become ceramic-enriched at the bottom, and based on different values of a, b, c and N, the material at the top surface can be ceramic, metal or a mixture of both. Fig. 2 better presents totally different attainable distributions of material properties across the thickness. During this study, the Poisson's ratio (v) is considered to be constant across the thickness.

Geometry of the shell is discretized using degenerated 8-noded shell elements based on the Mindlin-Reissner shell theory, which includes shear deformation effects. This element was proved to
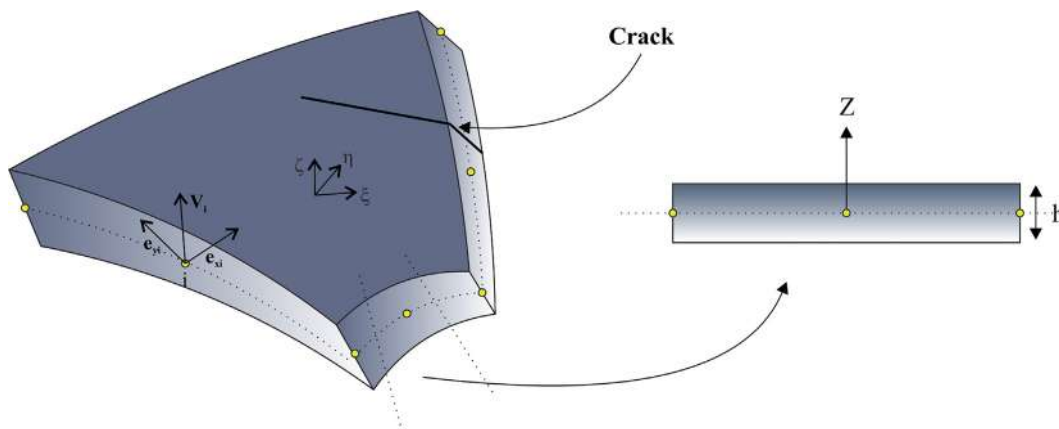

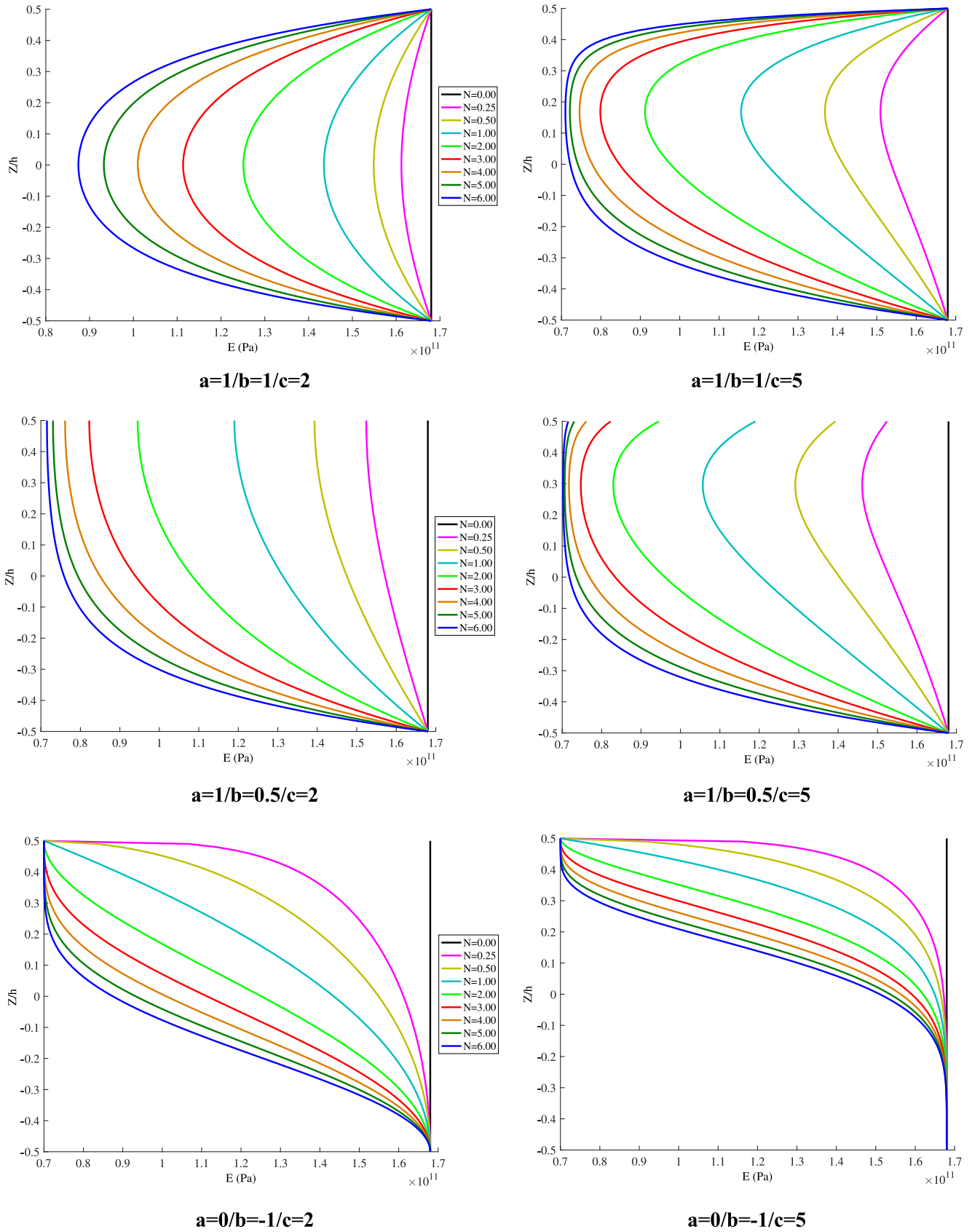**Fig. 1.** Geometry of an 8-noded cracked FGM shell element.

Fig. 2. Different FGM distribution profiles across the thickness of shell.

be efficient and reliable to address the conventional fracture problem of shells and plates [38,54],

$$\begin{Bmatrix} x \\ y \\ z \end{Bmatrix} = \sum_{i=1}^{8} N_i \begin{Bmatrix} x_i \\ y_i \\ z_i \end{Bmatrix} + \sum_{i=1}^{8} \frac{h_i \zeta_i}{2} \begin{Bmatrix} V_{xi} \\ V_{yi} \\ V_{zi} \end{Bmatrix}, \quad \mathbf{x} = \{x, y, z\}^T \tag{3}$$

where N_i's are the conventional finite element shape functions for eight noded elements, h_i is the shell thickness at node i, V_{ji}'s are the components of the normal vector V_i which is perpendicular to the shell surface at each node i and ζ_i, which is perpendicular to the shell mid-surface, is measured in the natural coordinate system, as shown in Fig. 1.

Approximation of the displacement $\mathbf{u}$ for a cracked FGM shell (Fig. 1) is composed of the conventional finite element approximation and the Heaviside enrichment for considering the displacement discontinuity across the crack,

$$\mathbf{u} = \mathbf{u}_{\text{Conventional FEM}} + \mathbf{u}_{\text{Heaviside enrichment}}; \quad \mathbf{u} = \{u, v, w\}^T \tag{4}$$

$$\begin{Bmatrix} u \\ v \\ w \end{Bmatrix} = \underbrace{\sum_{i=1}^{8} N_i \begin{Bmatrix} u_i \\ v_i \\ w_i \end{Bmatrix} + \sum_{i=1}^{8} \frac{t_i \zeta_i}{2} N_i \left(\beta_i \begin{Bmatrix} e_{y1}^i \\ e_{y2}^i \\ e_{y2}^i \end{Bmatrix} - \alpha_i \begin{Bmatrix} e_{x1}^i \\ e_{x2}^i \\ e_{x3}^i \end{Bmatrix} \right)}_{\mathbf{u}_{\text{Conventional FEM}}}$$
$$+ \underbrace{\sum_{i=1}^{8} N_i \mathbf{H}_i(\mathbf{x}) \begin{Bmatrix} a_{ix} \\ a_{iy} \\ a_{iz} \end{Bmatrix} + \sum_{i=1}^{8} \frac{t_i \zeta_i}{2} N_i \mathbf{H}_i(\mathbf{x}) \left(a_{i\beta} \begin{Bmatrix} e_{y1}^i \\ e_{y2}^i \\ e_{y2}^i \end{Bmatrix} - a_{i\alpha} \begin{Bmatrix} e_{x1}^i \\ e_{x2}^i \\ e_{x3}^i \end{Bmatrix} \right)}_{\mathbf{u}_{\text{Heaviside enrichment}}} \tag{5}$$

where u, v and w are the displacement components, corresponding to x, y and z directions, respectively. e_{xj}^i and e_{yj}^i are unit orthonormals vectors of the normal unit vector V at node i. α_i and β_i are the rotational degrees of freedom at node i with respect to x and y directions, respectively. Also, $\mathbf{H}_i(\mathbf{x})$ is the Heaviside function which is defined as [55]

$$H(\mathbf{x}) = \begin{cases} +1 & \mathbf{x} \text{ above the crack} \\ -1 & \mathbf{x} \text{ under the crack} \end{cases} \tag{6}$$

In Eq. (5), a_{ik}'s are the spurious degrees of freedom which are necessary to be considered in XFEM formulation and are added to the main degrees of freedom,

$$\mathbf{d} = \{u, v, w, \alpha, \beta\}^T \tag{7}$$

$$\mathbf{h} = \{a_x, a_y, a_z, a_\alpha, a_\beta\}^T \tag{8}$$

and the vector of degrees of freedom is composed of $\mathbf{d}$ and $\mathbf{h}$

$$\mathbf{D} = \{\mathbf{d} \quad \mathbf{h}\}^T \tag{9}$$

Previous studies [38,56] have shown that in eigenvalue problems such as buckling and vibration, the overall response of plate/shell is minimally affected by the existence of the crack tip enrichments. Hence, in the present study, the crack tip enrichment is discarded from the displacement approximation of $\mathbf{u}$.

The total potential energy ($\prod$) is composed of the elastic strain energy (U) and kinetic energy (T) of the system,

$$\prod = U + T \tag{10}$$
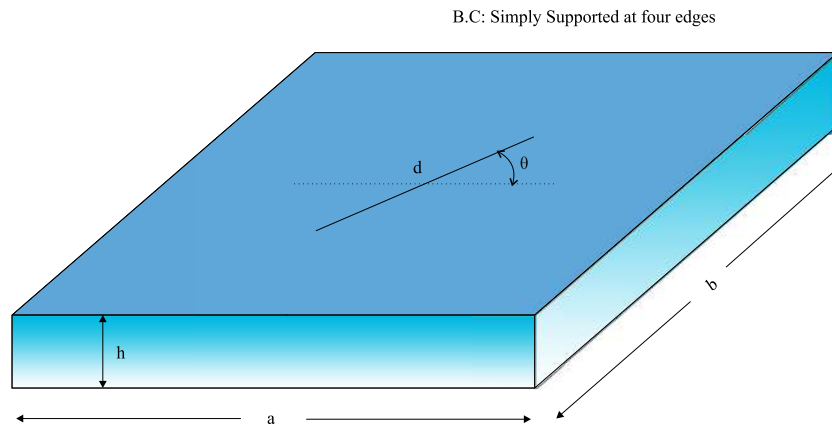
B.C: Simply Supported at four edges

Fig. 3. Simply supported cracked FGM rectangular plate.

Table 1
Normalized frequency parameters $\omega(b^2/h)\sqrt{\rho_c/E_c}$ for a simply supported horizontally cracked isotropic rectangular plate ($a/b = 2$, $b/h = 100$, $d/a = 0.5$).

Mode	Analytical [24]	Ritz method [20]	Ritz method [58]	XFEM [51]	Present study
1	3.050	3.053	3.047	3.055	3.052
2	5.507	5.506	5.503	5.508	5.506
3	5.570	5.570	5.557	5.665	5.559
4	9.336	9.336	9.329	9.382	9.357
5	12.760	12.780	12.760	12.861	12.785

Table 2
First normalized natural frequencies $\omega(b^2/h)\sqrt{\rho_c/E_c}$ for the simply supported cracked $FGM_{(a=1/b=0/c=0/N=1)}$ square plate ($\rho_m = 8166\,kg/m^3$, $E_m = 201\,GPa$, $\rho_c = 2370\,kg/m^3$, $E_c = 201\,GPa$, $v = 0.28$).

$\theta°$	XFEM [51]			Present study		
	$d/a = 0.4$	$d/a = 0.6$	$d/a = 0.8$	$d/a = 0.4$	$d/a = 0.6$	$d/a = 0.8$
0	3.04	2.86	2.75	3.04	2.86	2.75
10	3.04	2.85	2.73	3.04	2.85	2.73
20	3.03	2.83	2.68	3.03	2.84	2.67
30	3.03	2.81	2.62	3.03	2.81	2.62
40	3.02	2.79	2.58	3.02	2.80	2.59
45	3.02	2.79	2.57	3.02	2.80	2.56
50	3.02	2.79	2.58	3.02	2.80	2.59
60	3.03	2.81	2.62	3.03	2.81	2.62
70	3.03	2.83	2.68	3.03	2.84	2.67
80	3.04	2.85	2.73	3.04	2.85	2.73
90	3.04	2.86	2.75	3.04	2.86	2.75

Fig. 4. FGM circular plate with four radial cracks.

$$U = \frac{1}{2}\int_v \varepsilon^T \mathbf{C}\varepsilon dV \tag{11}$$

$$T = \frac{1}{2}\int_v \dot{\mathbf{u}}^T \rho_z \dot{\mathbf{u}} \cdot dV \tag{12}$$

where ε and $\mathbf{C}$ are the strain and the material property tensors. ε is related to the stress tensor σ by:

$$\sigma = \mathbf{C}\varepsilon \tag{13}$$

$$\mathbf{C} = \frac{E_z}{1-v^2}\begin{bmatrix} 1 & v & v & 0 & 0 & 0 \\ v & 1 & v & 0 & 0 & 0 \\ v & v & 1 & 0 & 0 & 0 \\ 0 & 0 & 0 & \frac{1-v}{2} & 0 & 0 \\ 0 & 0 & 0 & 0 & \frac{1-v}{2} & 0 \\ 0 & 0 & 0 & 0 & 0 & \frac{1-v}{2} \end{bmatrix} \tag{14}$$

$$\varepsilon = \left\{ \frac{\partial u}{\partial x}, \frac{\partial v}{\partial x}, \frac{\partial w}{\partial x}, \frac{\partial u}{\partial y} + \frac{\partial v}{\partial x}, \frac{\partial v}{\partial y}, \frac{\partial v}{\partial z} + \frac{\partial w}{\partial y}, \frac{\partial u}{\partial z} + \frac{\partial w}{\partial x} \right\}^T \tag{15}$$

Eqs. (11) and (12) can be rewritten as [51]

$$U = \frac{1}{2}\int_v \mathbf{D}^T \mathbf{B}^T \mathbf{C}\mathbf{B}\mathbf{D}dV \tag{16}$$

$$T = \frac{1}{2}\int_v \dot{\mathbf{D}}^T \mathbf{N}^T \rho_z \mathbf{N}\dot{\mathbf{D}}dV \tag{17}$$

where $\mathbf{N}$ and $\mathbf{B}$ are the matrices which include the shape functions and their derivatives, respectively. In the state of equilibrium, the first variation of potential energy must be equal to zero [51],

$$\delta\prod = \frac{\partial[U+T]}{\partial\mathbf{D}}\delta\mathbf{D} = \left\{ \left(\int_v \mathbf{B}^T\mathbf{C}\mathbf{B}dV\right)\mathbf{D} + \left(\int_v \rho_z\mathbf{N}^T\mathbf{N}dV\right)\ddot{\mathbf{D}} \right\}$$
$$\delta\mathbf{D} = 0 \quad \forall\mathbf{D}\neq 0 \tag{18}$$

So,

$$\mathbf{K}\mathbf{D} + \mathbf{M}\ddot{\mathbf{D}} = 0 \tag{19}$$

where $\mathbf{K}$ and $\mathbf{M}$ are the stiffness and mass matrices, respectively. Following a standard procedure [51,57], the second derivative of

Table 3
The first ten frequencies ($\omega/2\pi$) of the uncracked FGM circular plate for different power indices (clamped at $R = R_2$ and free at $R = R_1$).

Mode	$FGM_{(a=0/b=-0.5/c=2)}$				$FGM_{(a=1/b=0/c=0)}$			
	N = 0.6		N = 5.0		N = 0.6		N = 5.0	
	GDQ [59]	Present study	GDQ [59]	Present study	GDQ [60]	Present study	GDQ [60]	Present study
1	69.2	69.2	66.7	66.3	67.1	66.9	69.6	69.5
2	125.9	126.1	120.8	120.7	122.1	121.7	126.5	126.0
3	125.9	126.1	120.8	120.7	122.1	121.7	126.5	126.0
4	209.9	208.9	201.6	200.5	203.7	202.9	210.9	209.3
5	209.9	208.9	201.4	200.5	203.6	202.9	210.9	209.3
6	293.4	292.6	281.4	280.4	284.6	282.8	294.5	289.9
7	312.9	312.4	300.3	298.9	303.7	303.4	314.1	312.6
8	312.9	312.4	300.3	298.9	303.7	303.4	314.1	312.6
9	352.1	348.7	337.9	335.2	341.8	339.6	353.1	351.5
10	352.1	348.7	337.9	335.2	341.8	339.6	353.1	351.5

D can be replaced by $\ddot{\mathbf{D}} = -\omega^2 \mathbf{D}$, where ω represents the natural frequencies of the system. Substituting it in Eq. (19), the following eigenvalue equation is obtained,

$$(\mathbf{K} - \omega^2 \mathbf{M})\mathbf{D} = 0 \qquad (20)$$

where, **D** defines the eigenvectors, i.e. vibration mode shapes, and ω represents the eigenvalues.

The discretized forms of **K** and **M** can be written as,

$$\mathbf{K}_{ij}^{rs} = \int_v (\mathbf{B}_i^r)^T \mathbf{C}(\mathbf{B}_j^s) dV \qquad (21)$$

$$\mathbf{M}_{ij}^{rs} = \int_v \rho_z (\mathbf{N}_i^r)^T \mathbf{N}_j^s dV; \quad (r, s = \mathbf{d}, \mathbf{h}) \qquad (22)$$

where,

Table 4
First natural frequencies ($\omega_1/2\pi$) of cracked FGM$_{(a=1/b=0.5/c=4/N=2)}$ circular plate for various crack lengths and angles.

| d (m)	$\theta = 0°$	$\theta = 10°$	$\theta = 15°$	$\theta = 20°$	$\theta = 25°$	$\theta = 30°$	$\theta = 35°$	$\theta = 40°$	$\theta = 45°$
0.5	66.51	65.97	65.63	65.45	65.30	65.212	65.12	65.02	65.12
0.6	65.62	64.96	64.51	64.43	64.25	64.15	64.05	64.16	64.08
0.7	64.82	64.04	63.49	63.18	62.95	63.00	62.89	62.80	62.91
0.8	64.36	63.49	62.88	62.71	62.47	62.53	62.41	62.33	62.26
0.9	64.18	63.28	62.65	62.30	62.06	61.94	61.84	61.77	61.72
1.0	63.84	62.85	62.17	61.82	61.59	61.49	61.41	61.36	61.36
1.1	63.56	62.46	61.74	61.41	61.22	61.16	61.12	61.10	61.09
1.2	63.19	61.83	61.08	60.89	60.81	60.86	60.99	61.01	61.03
1.3	62.94	61.42	60.73	60.62	60.63	60.74	60.86	60.94	60.96
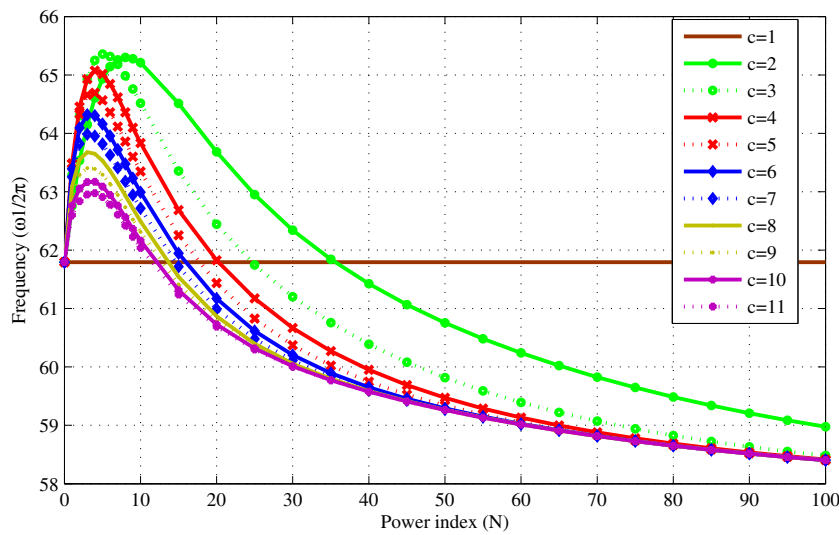
Fig. 5. First natural frequencies of FGM$_{(a=1/b=1/c/N)}$ circular plate with four radial cracks.
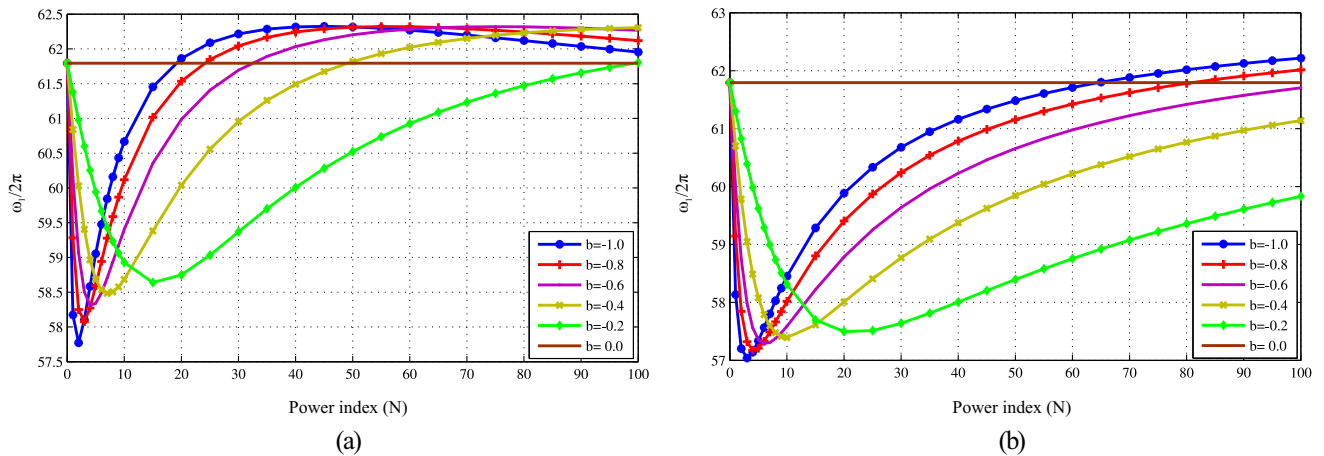

Fig. 6. First natural frequencies of a) FGM$_{(a=0/b/c=2/N)}$ b) FGM$_{(a=0/b/c=3/N)}$ circular plate with four radial cracks.
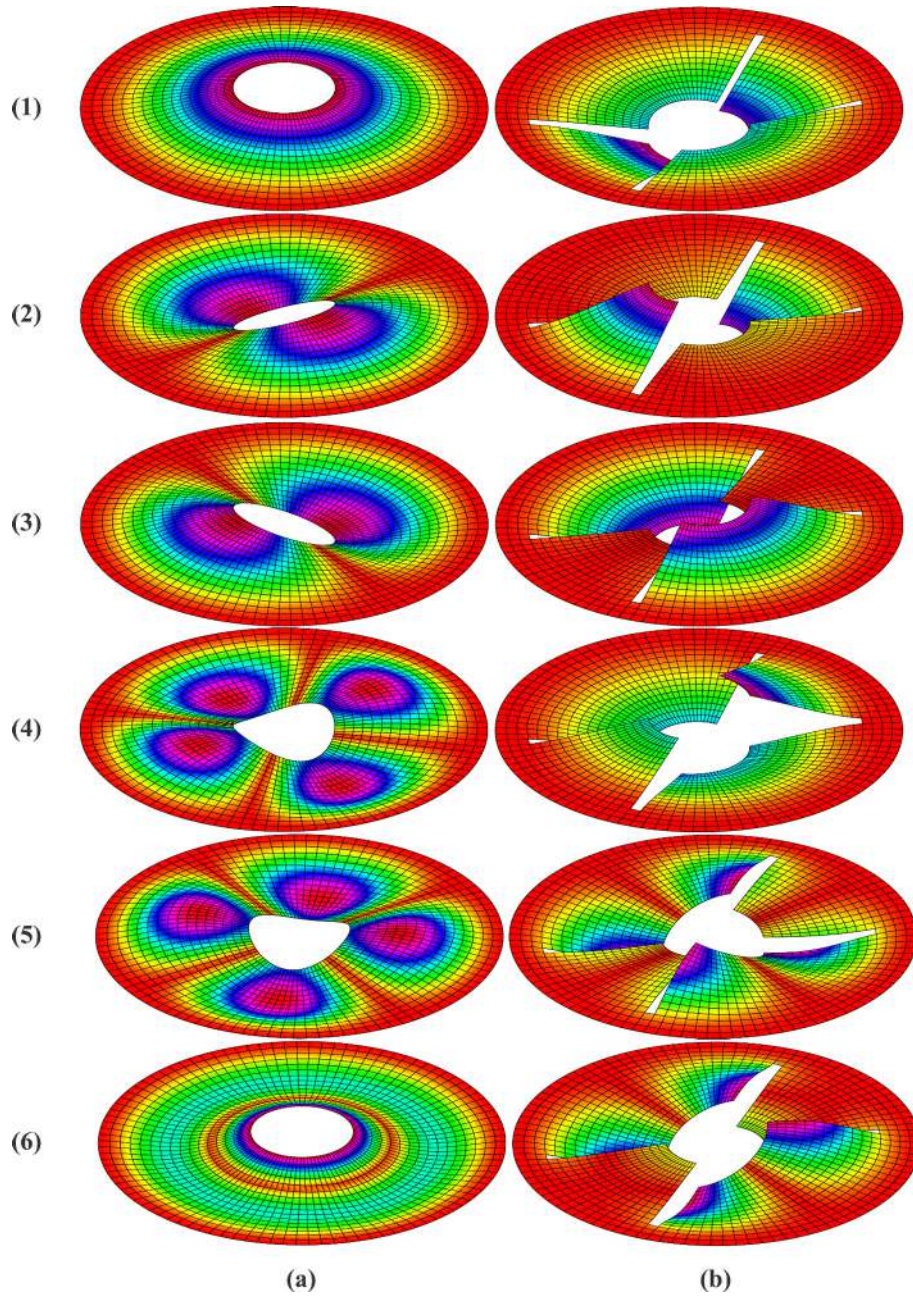
Fig. 7. The first six mode shapes of a) uncracked b) cracked FGM$_{(a=0/b=-0.4/c=2/N=15)}$ circular plate with $d = 1.2$ m and $\theta = 30°$.

$$\mathbf{B}_i^{\mathbf{d}} = \begin{bmatrix} N_{i,x} & 0 & 0 & \left(-\frac{\zeta_i t_i}{2} e_{x1}^i N_i\right)_{,x} & \left(\frac{\zeta_i t_i}{2} e_{y1}^i N_i\right)_{,x} \\ 0 & N_{i,y} & 0 & \left(-\frac{\zeta_i t_i}{2} e_{x2}^i N_i\right)_{,y} & \left(\frac{\zeta_i t_i}{2} e_{y2}^i N_i\right)_{,y} \\ 0 & 0 & N_{i,z} & \left(-\frac{\zeta_i t_i}{2} e_{x3}^i N_i\right)_{,z} & \left(\frac{\zeta_i t_i}{2} e_{y3}^i N_i\right)_{,z} \\ N_{i,y} & N_{i,x} & 0 & \left(-\frac{\zeta_i t_i}{2} e_{x1}^i N_i\right)_{,y} + \left(-\frac{\zeta_i t_i}{2} e_{x2}^i N_i\right)_{,x} & \left(\frac{\zeta_i t_i}{2} e_{y1}^i N_i\right)_{,y} + \left(\frac{\zeta_i t_i}{2} e_{y2}^i N_i\right)_{,x} \\ 0 & N_{i,z} & N_{i,y} & \left(-\frac{\zeta_i t_i}{2} e_{x2}^i N_i\right)_{,z} + \left(-\frac{\zeta_i t_i}{2} e_{x3}^i N_i\right)_{,y} & \left(\frac{\zeta_i t_i}{2} e_{y2}^i N_i\right)_{,z} + \left(\frac{\zeta_i t_i}{2} e_{y3}^i N_i\right)_{,y} \\ N_{i,z} & 0 & N_{i,x} & \left(-\frac{\zeta_i t_i}{2} e_{x1}^i N_i\right)_{,z} + \left(-\frac{\zeta_i t_i}{2} e_{x3}^i N_i\right)_{,x} & \left(\frac{\zeta_i t_i}{2} e_{y1}^i N_i\right)_{,z} + \left(\frac{\zeta_i t_i}{2} e_{y3}^i N_i\right)_{,x} \end{bmatrix} \quad (23)$$

$$\mathbf{N}_i^{\mathbf{d}} = \begin{bmatrix} N_i & 0 & 0 & -\frac{\zeta_i t_i}{2} e_{x1}^i N_i & \frac{\zeta_i t_i}{2} e_{y1}^i N_i \\ 0 & N_i & 0 & -\frac{\zeta_i t_i}{2} e_{x2}^i N_i & \frac{\zeta_i t_i}{2} e_{y2}^i N_i \\ 0 & 0 & N_i & -\frac{\zeta_i t_i}{2} e_{x3}^i N_i & \frac{\zeta_i t_i}{2} e_{y3}^i N_i \end{bmatrix} \quad (24)$$

For computing $\mathbf{B}_i^{\mathbf{h}}$ and $\mathbf{N}_i^{\mathbf{h}}$, N_i terms should be replaced by $N_i(H(\mathbf{x}) - H(\mathbf{x}_i))$ in Eqs. (23) and (24).

It is inevitable to employ numerical integration for assessing the values of Eqs. (21) and (22) properly. Based upon the fact that the existence of crack complicates the displacement field, the conventional Gauss quadrature integration cannot be simply adopted to evaluate the integrals. In this study, the sub-triangulation method is employed to integrate over the elements which contain the crack path and 7 Gauss points per triangle are considered [54]. For uncracked elements, a 2×2 Gauss quadra-

ture rule is adopted. Also, 8 Gauss points are considered to integrate across the thickness of shell. It should be mentioned that no blending elements are considered in the present study, as it has a non-essential effect in eigenvalue analysis of plates and shells [38,39].

3. Numerical simulations

In this section, the proposed XFEM formulation is verified for vibration analysis of cracked isotropic and FGM plates with limited available reference results. Then, the method is employed for computing the natural frequencies and mode shapes of cracked FGM plates and shells. Four examples are presented and the effects of crack length, crack angle and material distribution across the thickness of shell are extensively studied. In all examples, the following material properties are considered: $E_m = 70$ GPa, $\rho_m = 2707$ Kg/m^3, $E_c = 168$ GPa and $\rho_c = 5700$ Kg/m^3 (unless explicitly mentioned otherwise).

3.1. Cracked isotropic and FGM rectangular plates

The problem of vibration analysis of a cracked rectangular plate (Fig. 3) has been studied by many researchers [20,24,51,58]. Here, the natural frequencies for two cases of isotropic and FGM simply supported plates are obtained and compared with the available results. A 25×25 structured mesh is adopted for performing the analysis.

The first five normalized natural frequencies for the cracked isotropic rectangular plate are presented in Table 1. A very good agreement is observed with available references.

Also, the first normalized natural frequencies of the cracked FGM plate for different crack lengths and orientations are presented in Table 2. It can be seen that the frequencies decrease as the crack length increases. Also, with increasing the crack angle, initially the natural frequencies decrease up to $\theta = 45°$ and then increase until the crack angle reaches to $\theta = 90°$. Moreover, a very good agreement is observed between the present results and those reported by Natarajan et al. [51].
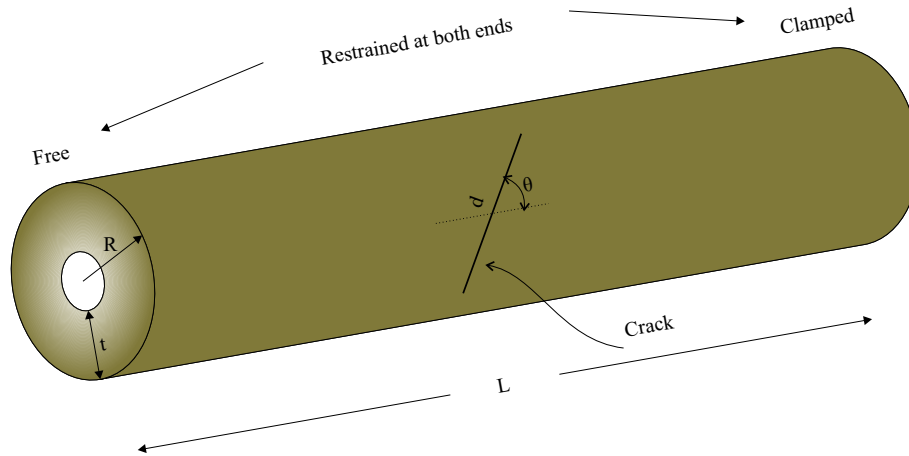

Fig. 8. Geometry of the cracked FGM cylindrical shell.

Table 5
First ten natural frequencies $(\omega/2\pi)$ of uncracked FGM$_{(a=1/b=0.5/c=2/N)}$ cylindrical shell for various power indices and clamped-free boundary conditions.

Mode	$N = 0.6$				$N = 20$			
	GDQ [59]	Analytical [61]	Analytical [62]	Present study	GDQ [59]	Analytical [61]	Analytical [62]	Present study
1	152.3	152.0	151.1	152.2	146.5	146.2	145.3	146.4
2	152.3	152.0	151.1	152.2	146.5	146.2	145.3	146.4
3	219.9	219.5	218.9	219.8	215.9	215.5	215.0	215.6
4	219.9	219.5	218.9	219.8	215.9	215.5	215.0	215.6
5	252.2	251.9	252.3	251.9	239.8	239.5	239.9	239.2
6	252.2	251.9	252.3	251.9	239.8	239.5	239.9	239.2
7	383.4	382.9	383.6	383.3	377.3	376.7	377.6	376.9
8	383.4	382.9	383.6	383.3	377.3	376.7	377.6	376.9
9	417.7	417.7	417.6	417.6	396.8	396.7	396.6	396.7
10	430.0	429.5	426.6	429.6	417.2	416.6	413.9	416.8

Table 6
First natural frequencies $(\omega_1/2\pi)$ of cracked FGM$_{(a=1/b=0.5/c=2/N=2)}$ cylinder for various crack lengths and angles.

d/R	$\theta = 0°$	$\theta = 15°$	$\theta = 30°$	$\theta = 45°$	$\theta = 60°$	$\theta = 75°$	$\theta = 90°$
0.5	**381.79**	382.53	381.69	380.78	378.80	379.42	**375.53**
0.8	375.76	375.22	372.86	373.01	374.72	354.37	355.26
1.0	375.78	375.24	372.86	365.03	356.91	354.06	336.68
1.2	369.87	369.35	370.25	365.03	344.34	317.42	290.08
1.5	**368.58**	367.96	366.93	355.28	329.97	278.17	**248.57**

3.2. FGM circular plate with four radial cracks

Circular plates are frequently used as grinding disks or cutters in industry and because such processes produce large amounts of heat, FGM disks are potentially an appropriate option. In this section, the first ten natural frequencies of an uncracked FGM circular plate are determined for different power indices (N), and then the results are compared with the available Refs. [59,60]. Then, the section is further extended to comprehensively study the vibrational behavior of FGM circular plates with four radial cracks (Fig. 4). Geometric properties of the plate are: $R_2 = 2$ m, $R_1 = 0.5$ m and $t = 0.1$ m. The plate is clamped and free at $R = R_2$ and $R = R_1$ boundaries, respectively. Moreover, it is intended to investigate how different variables such as crack length and orientation and FGM properties (a, b, c and N) can affect the fundamental natural frequencies.

The first ten frequencies of the uncracked functionally graded circular plate with two different material distributions across the thickness of the plate are obtained and compared with the results of Refs. [59,60] in Table 3, which shows a very close agreement.

Now, the proposed XFEM formulation is employed to study the vibration behavior of FGM circular plate with four radial cracks. The fundamental natural frequencies for various crack lengths

and orientations for the FGM$_{(a=1/b=0.5/c=4/N=2)}$ circular plate are provided in Table 4. It is observed that the plate is affected by the variations of the crack length; its natural frequencies are reduced as the crack length increases, though it is not a significant change. For example, changing the length of the cracks from $d = 0.5$ m to $d = 1.3$ m causes only a reduction of 6.3% in the natural frequency (related to the crack angle of $\theta = 45°$). Likewise, the vibrational behavior of the plate is not substantially affected by the crack orientations such that a maximum reduction of 3.3% is observed in the natural frequencies of the plate with $d = 1.3$ m when the angles of the cracks change from $\theta = 0°$ to $\theta = 45°$.

The effect of FGM distribution parameters such as b, c and N on the vibrational behavior of the plate for the case of $d = 1.2$ m and $\theta = 30°$ are shown in Figs. 5 and 6. Sensitivities of frequencies to the parameter c and power index N are depicted in Fig. 5. It can be seen that with increasing c, the natural frequencies decrease, while with increasing the power indices (N), the frequencies initially increase and then decrease.

Fig. 6 shows the vibrational response of the cracked FGM circular plate for different values of b and power indices (N) for two cases of $c = 2$ and $c = 3$. It is observed that the frequencies experience a steep drop and then increase as the power indices increase.
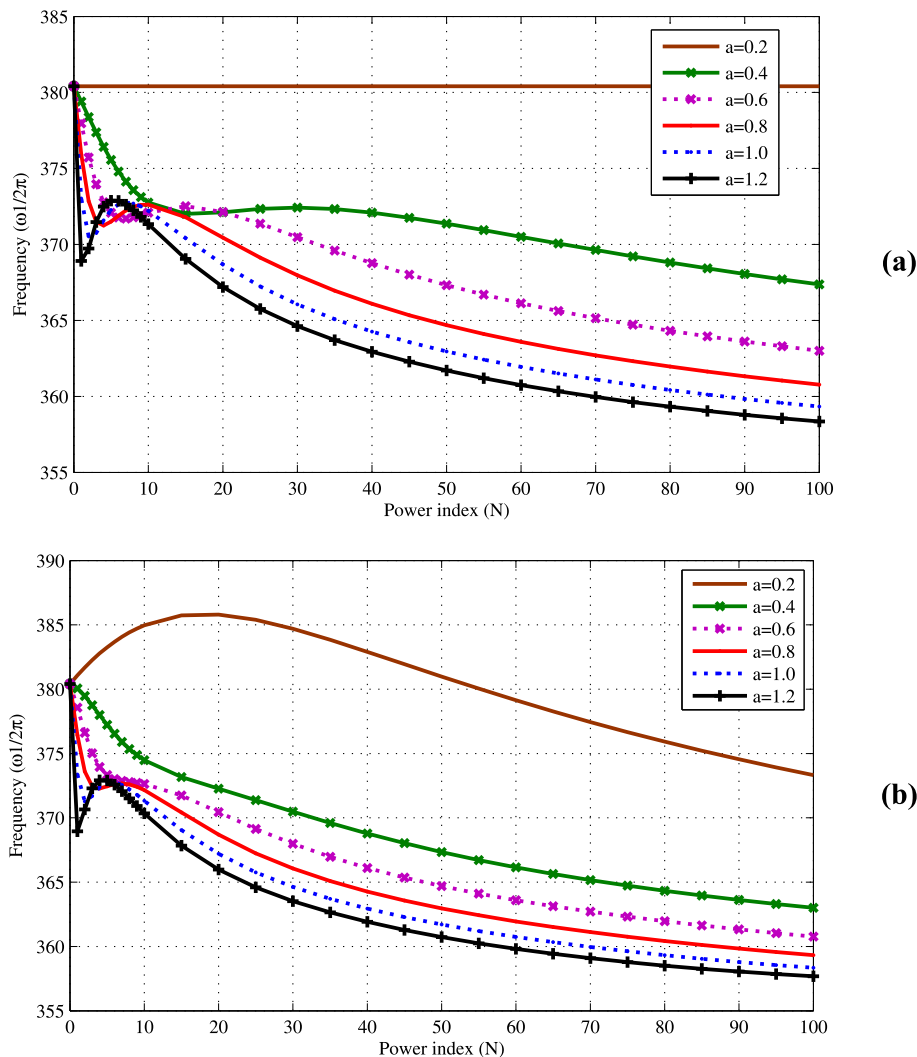

Fig. 9. First natural frequencies of cracked cylindrical shell a) FGM$_{(a/b=0.2/c=1/N)}$ b) FGM$_{(a/b=0.2/c=3/N)}$.
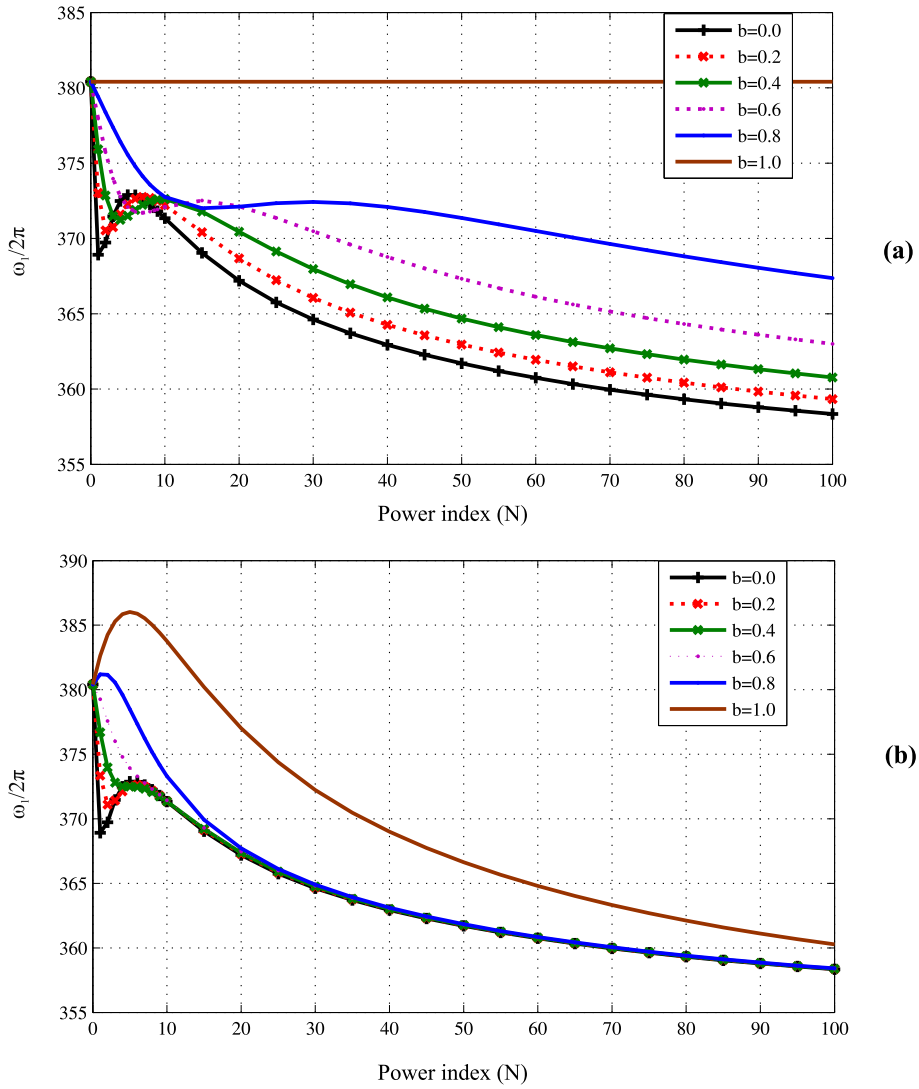
(a)

(b)

Fig. 10. First natural frequencies of cracked cylindrical shell a) FGM$_{(a=1/b/c=1/N)}$ b) FGM$_{(a=1/b/c=2/N)}$.
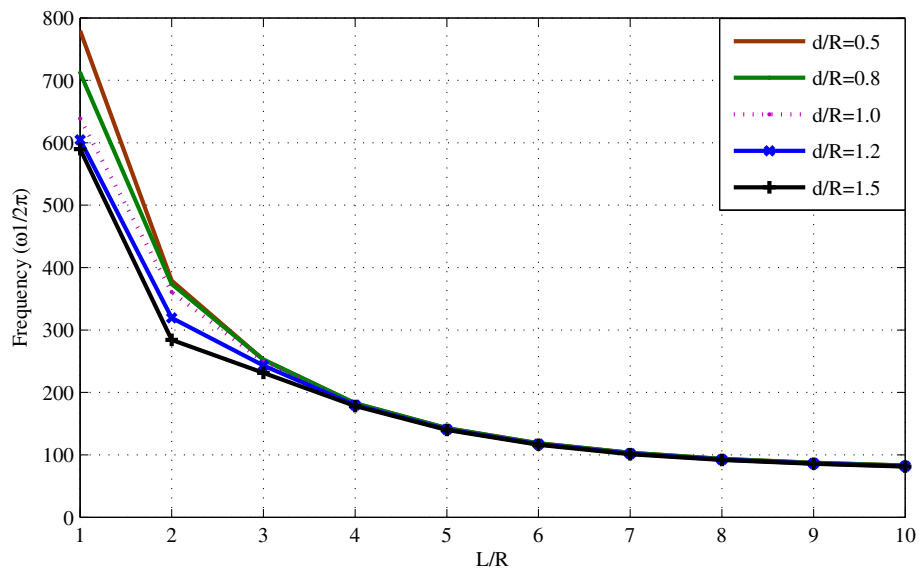

Fig. 11. Effect of L/R and d/R on the first natural frequencies of the cracked FGM$_{(a=1/b=0.5/c=2/N=3)}$ cylindrical shell.

In general and based upon the highly complex vibrational behavior of the problem, a definite conclusion cannot be made for the general effect of different FGM profiles across the thickness of the plate.

Fig. 7 provides further insight into the effects of cracks on the vibration mode shapes of the circular plate. It can be seen that the presence of cracks makes the FGM plate to vibrate in a different manner in comparison to the intact plate.

3.3. Cracked FGM cylindrical shell

FGM cylindrical shells are widely utilized in aerospace, marine and other engineering fields. Prime examples include fuel nozzles in aircrafts and formula 1 cars. In this example, vibration analysis for a perfect FGM cylindrical shell is performed and the obtained results are compared with available reference results. Then, the vibrational behavior of the cracked functionally graded cylindrical
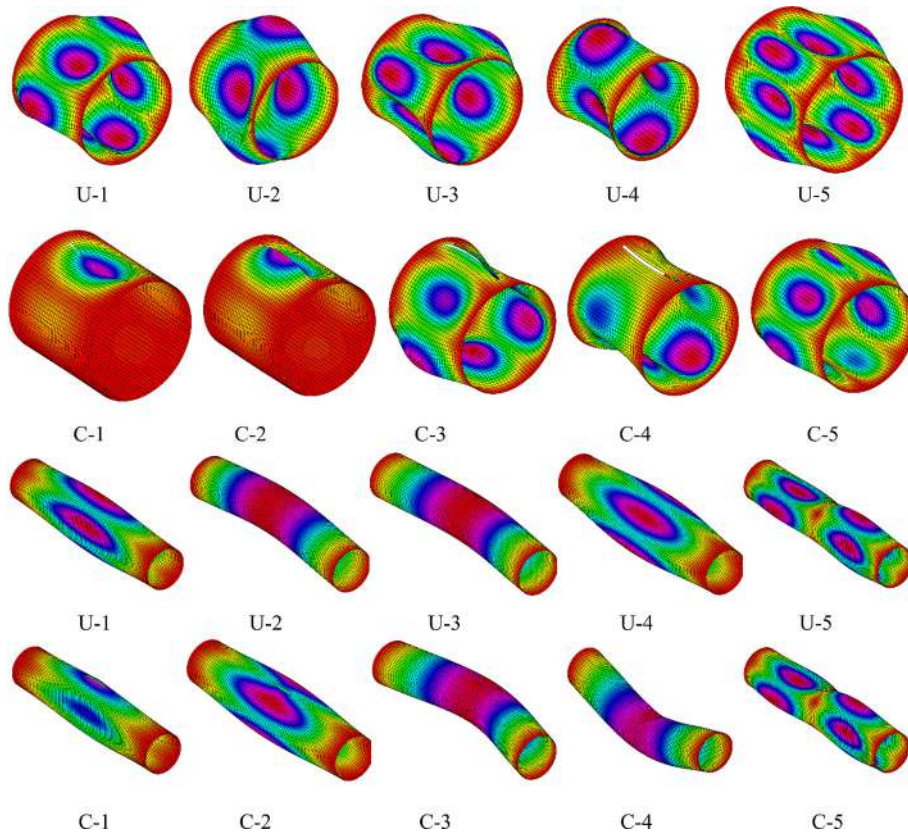

Fig. 12. First five mode shapes of uncracked (U) cracked (C) and $FGM_{(a=1/b=0.5/c=2/N=3)}$ cylindrical shells for two cases of $L/R = 2$ and $L/R = 10$ with $d/R = 1.5$ and $\theta = 90°$.
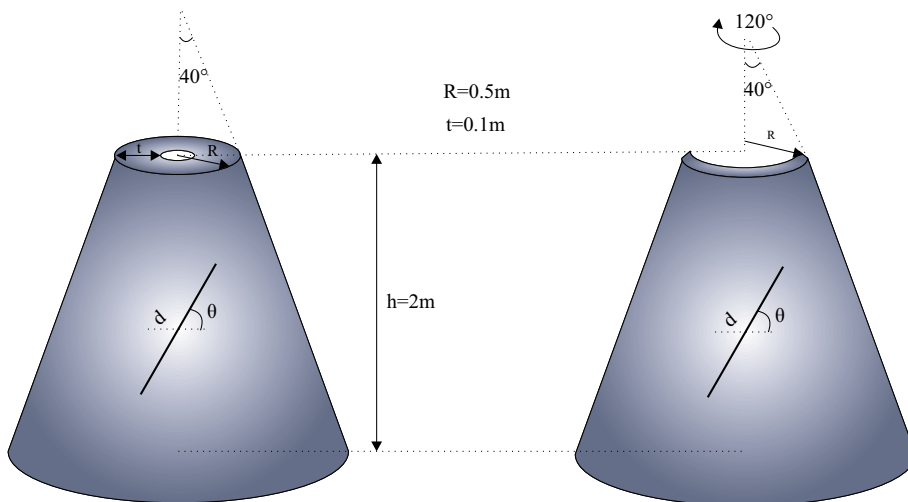

Fig. 13. Geometry of the cracked FGM conical dome and panel.

shell, as depicted in Fig. 8, is extensively investigated and the effects of different parameters such as crack length and angle, cylinder length and FGM profile parameters (a, b, c, N) on the fundamental frequencies are examined. The following geometric properties are considered for all the analyses: $L = 2$ m, $R = 1$ m and $t = 0.1$ m. A structured 35×35 (in circumferential and longitudinal directions) mesh is adopted (unless mentioned otherwise).

For an uncracked $\text{FGM}_{(a=1/b=0.5/c=2/N)}$ cylindrical shell with clamped boundary condition at one end and free at the other, vibration analysis is carried out and the first ten natural frequencies are determined and compared with available references in Table 5. It is observed that the frequencies obtained in the present study are completely consistent with those reported by other researchers [59,61,62]. The method is clearly reliable to be employed for vibration analysis of more complicated problems such as cracked functionally graded cylindrical shells.

Table 6 presents the effects of crack length and angle on the natural frequencies of the cracked FGM cylindrical shell. First of all, with increasing ratio of crack length to radius, the natural frequency decreases. It is noted that this reducing trend is more tangible for the cases where the crack angle is $\theta = 90°$. For instance, the frequency is reduced by 51.2% when the crack length to radius ratio (d/R) increases form 0.5 to 1.5 for the longitudinal crack orientation case $(\theta = 90°)$. Moreover, the natural frequency undergoes a significant drop when the crack angle increases form $0°$ to $90°$. Accordingly, when the crack orientation alters from the circumferential direction $(\theta = 0°)$ to the longitudinal direction $(\theta = 90°)$, the frequency of the shell attenuates by a factor of 48.3% for the $d/R = 1.5$ case.

For further investigation, the effects of FGM parameters (a, b, c, N) on the vibrational response of circumferentially cracked

$(\theta = 0°)$ FGM shell are demonstrated in Figs. 9 and 10. It is observed that any combination of FGM's distribution parameters (a, b, c, N) across the thickness of the shell contributes differently to the complex behavior of the model, making it extremely difficult to predict the general vibrational behavior of the cylinder.

Fig. 11 is presented to show how the ratios of cylinder length to radius (L/R) can affect the fundamental frequencies of the circumferentially cracked FGM cylindrical shell for various crack length to radius ratios. It can be seen that the natural frequencies decrease dramatically when the cylinder length to the radius ratios increase. Accordingly, the frequency associated with $L/R = 1$ is approximately 7 times greater than the one associated with $L/R = 10$ for the $d/R = 0.5$ case. In addition, with increasing the L/R ratios, the effect of crack length on the vibrational behavior of the shell gradually fades. The reason can be attributed to the fact that for high L/R ratios, the global vibrational mode is dominant and the existence of a small crack cannot drastically influence such global response.

Fig. 12 presents the effects of the existence of crack as well as the length of the shell on the vibration mode shapes for the $\text{FGM}_{(a=1/b=0.5/c=2/N=3)}$ cylindrical shell. It is observed that for the case of $L/R = 2$ the vibrational behavior is significantly affected by the presence of crack and the vibration mode shapes are totally different for intact and cracked shells. Nevertheless, the vibrational behavior of relatively long cylinders $(L/R = 10)$ is not drastically disturbed by the existence of crack.

3.4. Cracked FGM conical shells

Similar to FGM cylindrical shells and to a higher extent, functionally graded conical shells are widely used in the aerospace industry. Vibration analysis of cracked FGM conical panels and domes, as shown in Fig. 13, is now considered. First, a convergence

Table 7
The first five frequencies ($\omega/2\pi$) of the uncracked FGM conical shells for different power indices.

| | Mode | $\text{FGM}_{(a=1/b=0.5/c=2)}$ | | | | $\text{FGM}_{(a=1/b=0/c=0)}$ | | | |
| | | $N = 0.6$ | | $N = 20$ | | $N = 0.6$ | | $N = 20$ | |
		Analytical [59]	Present study	Analytical [59]	Present study	Analytical [60]	Present study	Analytical [60]	Present study
Conical panel	1	80.1	80.0	77.8	77.5	78.2	78.2	77.8	77.6
	2	110.9	109.5	106.7	106.3	109.0	108.9	106.7	106.1
	3	158.6	155.0	153.9	151.7	154.9	153.6	153.8	152.9
	4	195.2	194.9	190.4	188.7	189.6	188.2	190.3	189.1
	5	259.1	256.4	250.8	247.1	253.4	251.3	250.7	248.9
Conical dome	1	208.9	208.9	204.9	204.8	205.9	205.8	200.8	200.7
	2	208.9	208.9	204.9	204.8	205.9	205.8	200.8	200.7
	3	230.1	228.5	227.3	226.1	225.5	224.7	224.3	224.0
	4	230.1	228.5	227.3	226.1	225.5	224.7	224.3	224.0
	5	284.7	282.1	282.7	281.5	277.9	276.5	280.1	278.3

Table 8
First natural frequencies ($\omega_1/2\pi$) of cracked $\text{FGM}_{(a=0/b=-0.5/c=2/N=5)}$ conical shell and panel for various crack lengths and angles.

	d	$\theta = 0°$	$\theta = 15°$	$\theta = 30°$	$\theta = 45°$	$\theta = 60°$	$\theta = 75°$	$\theta = 90°$
Conical dome	0.5	200.6	200.6	200.6	200.4	199.2	199.5	199.5
	0.7	200.7	200.6	200.5	200.2	199.1	197.0	197.2
	1.0	198.9	198.5	196.1	193.9	193.8	182.2	183.5
	1.2	196.9	196.1	191.1	186.6	185.6	176.1	171.7
	1.5	193.6	190.1	181.2	171.2	160.5	150.0	146.0
	1.6	193.6	183.3	172.2	161.7	151.4	142.7	135.1
Conical panel	0.5	285.1	284.4	284.6	284.1	293.4	283.2	284.1
	0.7	283.7	282.3	281.9	277.3	269.6	272.9	276.8
	1.0	278.5	276.2	266.9	259.8	249.3	233.6	234.7
	1.2	271.1	255.2	250.7	241.0	229.2	215.3	214.3
	1.5	245.5	246.5	230.6	211.5	202.8	189.2	185.5
	1.6	245.5	237.7	225.3	211.5	191.5	187.6	177.5

study is performed for the uncracked FGM conical shell and the results are compared with the reference results [59,60]. Then, vibrational behaviors of the cracked functionally graded conical panels and domes are further investigated. For the conical dome and panel, meshes with respectively 1225 and 525 shell elements are adopted.

The first five frequencies of the FGM conical specimens are presented in Table 7. The boundary condition of the conical panel is C-F-F-F (clamped at the bottom and free at the other edges) and the boundary condition of the conical dome is C-F (clamped at the bottom and free at the top). It is observed that the predicted natural frequencies for all vibration modes are in very close agreement with the reference results [59,60].

The section is now further extended to study the vibrational behavior of cracked functionally graded conical shells.

Table 8 presents the effect of crack length and angle on the fundamental natural frequency of cracked FGM conical shells. The boundary condition of the conical dome is C-F, while the boundary condition of the conical panel is C-C-C-C (clamped at all edges). Is it observed that the natural frequencies decrease when the crack angle increases. For example, for the conical dome, the frequency drops by 43.3% when the crack orientation increases from $0°$ to $90°$ for the $d = 1.6$ m case. The minimum values of the

frequencies are associated with the vertical crack direction ($\theta = 90°$). Also, the crack length affects the fundamental frequencies of both conical shells significantly. For example, the natural frequency related to the conical panel decreases by up to 60% when the crack length increases from $d = 0.5$ m to $d = 1.6$ m for the case in which the crack angle is $\theta = 90°$.

Fig. 14 compares the effects of FGM parameters a, c and N on the natural frequencies of cracked FGM conical shells (for $d = 1.5$ m and $\theta = 60°$). First of all, it is observed that the overall response of both conical shells for different variations of the parameters a, c, N is relatively similar. Nonetheless, there are differences in the values of the associated frequencies in both cases. Furthermore, the vibrational response of the shells for the initial power index values is somewhat unpredictable, whereas the responses follow a decreasing trend as the power index increases.

The first six vibration mode shapes for cracked and uncracked functionally graded conical shells are shown in Fig. 15. It is observed that the crack can significantly alter the vibrational behavior of the FGM conical shells from a global response to a more localized behavior.

To further examine the vibrational response of cracked FGM conical shells due to the variations of FGM parameters, the fundamental frequencies for various values of b, c and N for the
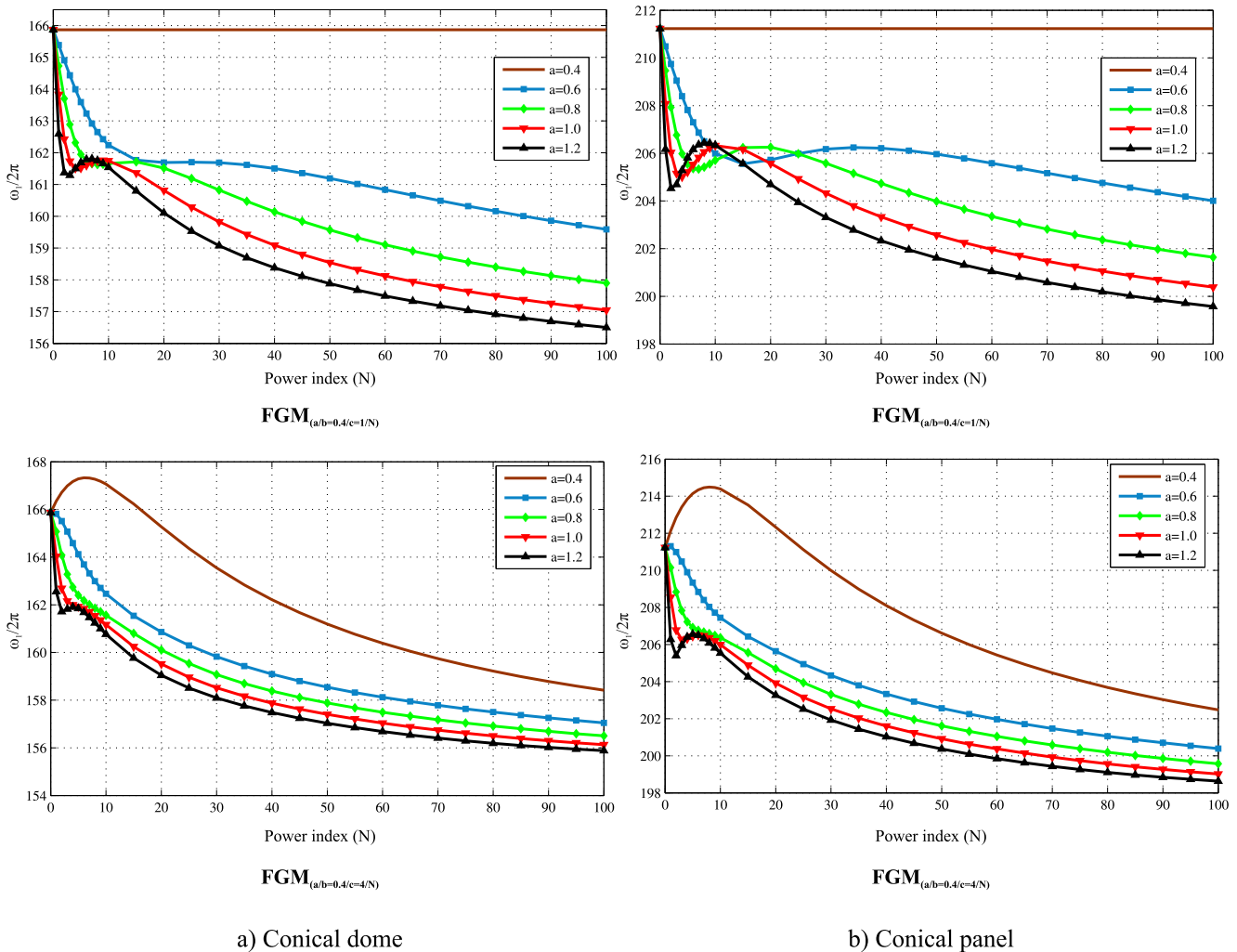

a) Conical dome

b) Conical panel

Fig. 14. Effects of parameters a, c and N on the first natural frequencies of cracked FGM a) conical domes and b) conical panels.
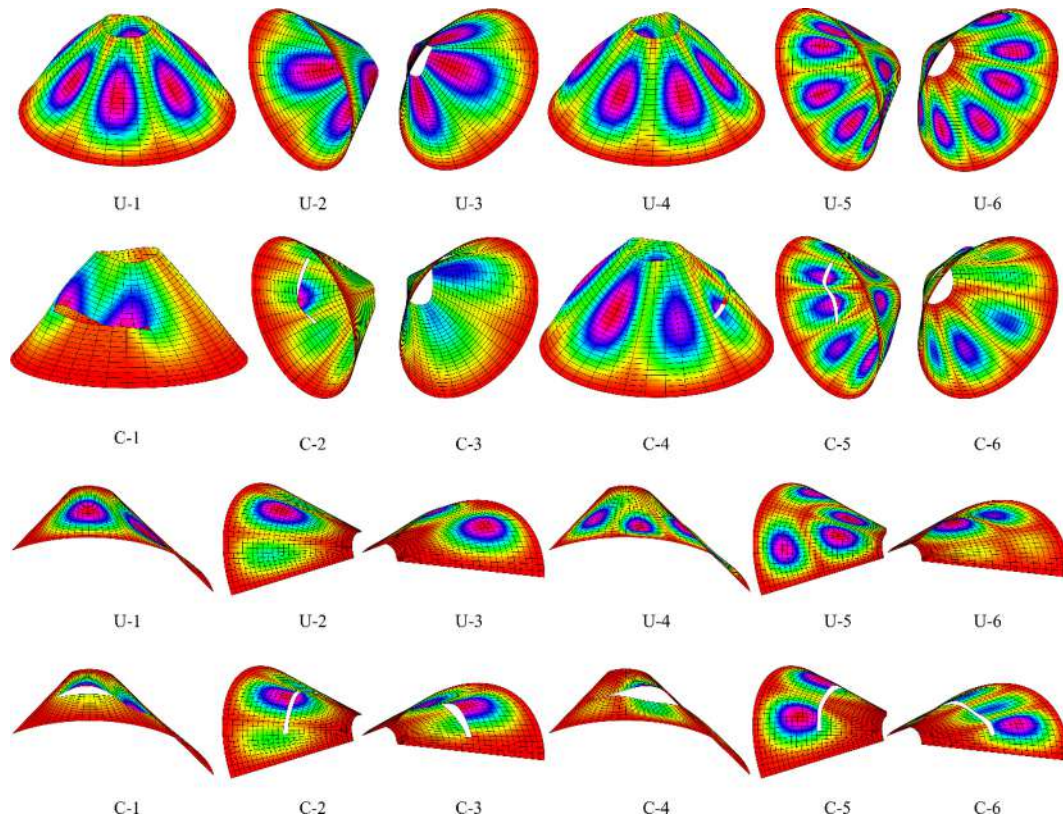
Fig. 15. The first six vibration mode shapes of uncracked (U) and cracked (C) FGM$_{(a=0/b=-0.5/c=2/N=5)}$ conical domes and panels with $d = 1.5$ m and $\theta = 0°$.

case of $d = 1.5$ m and $\theta = 60°$ are examined in Fig. 16. As mentioned before, due to the highly complex behavior of cracked FGM conical shells in different combinations of FGM parameters (a, b, c and N), it is a formidable task to, in general, predict the vibrational behavior and therefore a case by case analysis is always required.

3.5. Cracked FGM spherical dome

As the last example, vibration analysis of the cracked FGM spherical dome (Fig. 17) is carried out and the effects of various parameters like crack length and angle, as well as the FGM characteristic parameters (a, b, c and N), on the natural frequencies are comprehensively examined.

First, the vibration analysis is performed for the perfect FGM spherical dome and the effect of power index on the first ten natural frequencies is examined. Table 9 shows that the natural frequencies decrease with the increase of power indices. Moreover, the natural frequencies associated with higher modes of vibration are significantly greater than those of lower modes of vibration. For instance, the tenth natural frequency of the FGM dome is 1.92 times greater than the first frequency of the same dome for the case where $N = 0.5$.

The first eight vibration mode shapes of intact and cracked FGM spherical shells are depicted in Fig. 18. It is observed that the existence of crack completely alters the vibrational mode shapes of the sphere.

Fig. 19 illustrates the effects of crack length and orientation on the fundamental natural frequencies of cracked FGM spherical dome. It can be perceived that for small crack length to radius ratios, the effect of the crack angle is negligible, whereas for larger crack length to radius ratios, the natural frequencies are highly

affected by variations of the crack angle. Accordingly, the frequency corresponding to $\theta = 90°$ is 1.23 times smaller than the one corresponding to $\theta = 0°$ for the $d/R = 1.0$ case. In addition, the crack length to radius ratio has a considerable influence on the frequency of the sphere, such that a reduction of 50% is observed when the crack length to radius ratio grows from 0.5 to 1.5 for the $\theta = 90°$ case.

Now, the effects of FGM parameters (a, b, c and N) on the vibrational behavior of cracked spherical domes are investigated. Fig. 20 shows that based on different combinations of FGM parameters, the problem takes on different behaviors. For example, for the case of FGM$_{(a=1/b/c=1/N)}$, the natural frequency associated with $b = 0$ undergoes a decline then increases as the gradient index increases to $N = 5$. It decreases again and continues this trend, whereas for the case associated with $b = 0.95$, the frequency decreases continuously as the power index (N) increases.

4. Conclusion

A reliable and efficient shell formulation within the framework of the extended finite element method (XFEM) has been introduced and effectively utilized to analyze the vibrational behavior of cracked FGM shells. Through simulation of different problems, it has been proved that the proposed method can reliably address the problem of vibration analysis in FGM plate and shell structures. Then, the method has been employed to carry out the vibration analysis of five different cracked FGM problems including two plates and three shells. Throughout the study, comprehensive results concerning the vibrational behavior of different shell structures have been attained, which can be safely used in designing real world structures. In addition, some specific conclusions can be made:
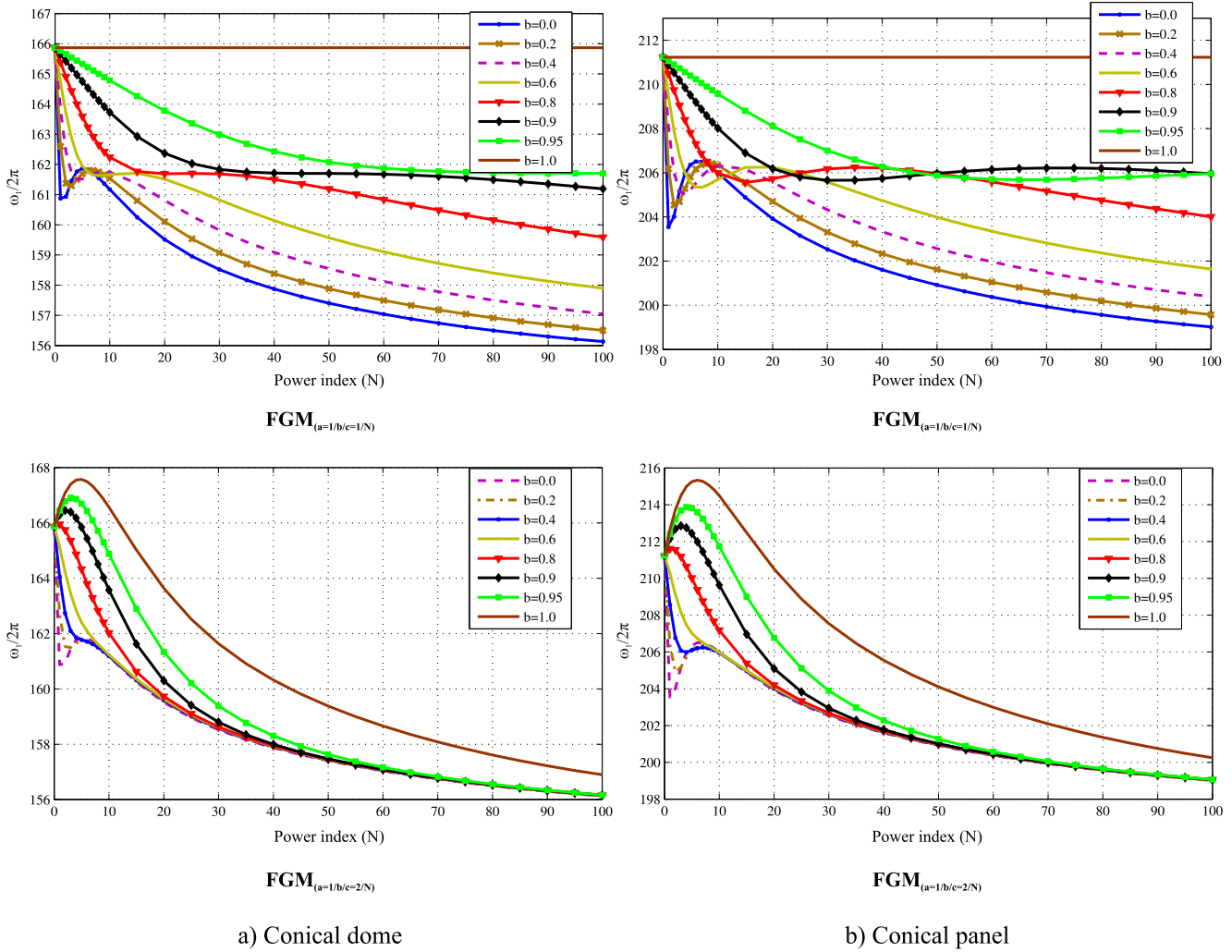
FGM$_{(a=1/b/c=1/N)}$

FGM$_{(a=1/b/c=1/N)}$

FGM$_{(a=1/b/c=2/N)}$

FGM$_{(a=1/b/c=2/N)}$

a) Conical dome

b) Conical panel

Fig. 16. Effects of parameters b, c and N on the first natural frequencies of cracked FGM a) conical domes and b) conical panels.
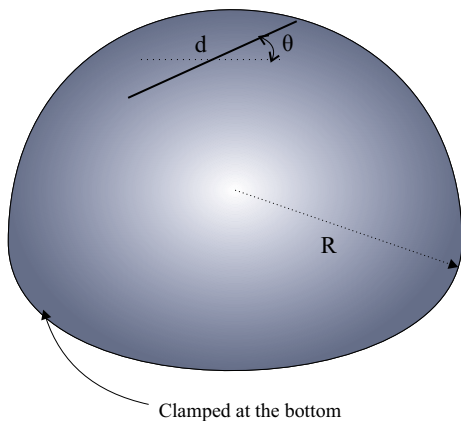

Clamped at the bottom

Fig. 17. Geometry of the cracked FGM spherical dome.

Table 9
The first ten natural frequencies ($\omega/2\pi$) of the uncracked FGM$_{(a=1/b=0.5/c=2/N)}$ spherical dome.

Mode	$N = 0.0$	$N = 0.5$	$N = 1.0$	$N = 2.0$	$N = 3.0$	$N = 4.0$	$N = 5.0$	$N = 6.0$
1	529.4	527.0	524.7	520.4	516.9	514.1	511.9	510.3
2	529.4	527.0	524.7	520.4	516.9	514.1	511.9	510.3
3	762.4	760.2	757.7	752.9	748.6	745.1	742.2	739.8
4	872.0	869.4	866.5	860.8	855.8	851.8	848.6	846.0
5	872.0	869.4	866.5	860.8	855.8	851.8	848.6	846.0
6	949.9	947.4	944.5	938.6	933.8	930.1	927.2	925.0
7	949.9	947.4	944.5	938.6	933.8	930.1	927.2	925.0
8	1015.4	1008.7	1002.0	991.4	983.0	976.8	972.2	968.9
9	1016.9	1014.3	1011.2	1004.9	999.8	996.0	993.2	990.9
10	1016.9	1014.3	1011.2	1004.9	999.8	996.0	993.2	990.9

- The fundamental natural frequency can be altered and affected by the angle of a crack in a dramatic fashion. As an example, the first natural frequency of the FGM conical dome plummets by almost 45% when the orientation of the crack rotates from $0°$ to $90°$.

- The vibrational mode shapes highly depend to the presence of the crack in the shell. Nonetheless, this dependency is more severe in some types of FGM shells than the others. For example, the mode shapes of cracked FGM spherical shells are thoroughly different from the intact ones.
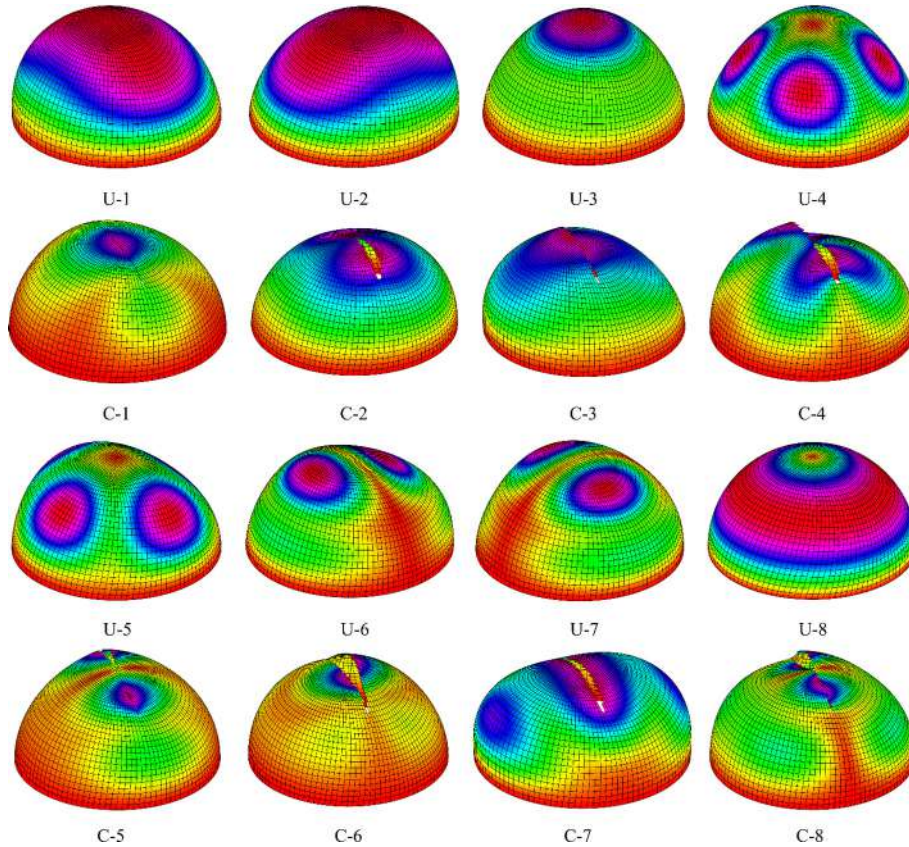
- Generally, the existence of cracks in the investigated examples can have a vital impact on the vibrational behavior of FGM shells. Nevertheless, there are also some types of structures that are minimally affected by the existence of cracks (FGM circular plates).

Fig. 18. The first eight vibration mode shapes of uncracked (U) and cracked (C) FGM$_{(a=1/b=0.5/c=2/N=3)}$ spherical domes with $d = 1.2\,\text{m}$ and $\theta = 85°$.
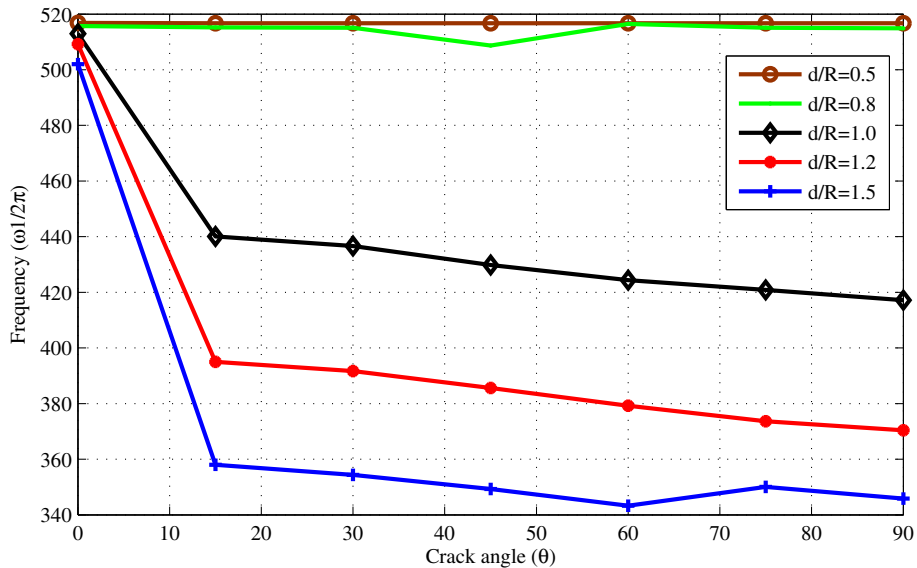

Fig. 19. Effects of crack length to radius ratio and crack angle on the first natural frequency of cracked FGM$_{(a=1/b=0.5/c=2/N=3)}$ spherical dome.

The FGM distribution parameters (a, b, c and N) are in the direct correlation with the fundamental natural frequencies of different shell structures such that even a small change in each of these parameters can yield in a fundamentally complex vibrational behavior, which generally makes the behavior of structure extremely difficult to foresee.
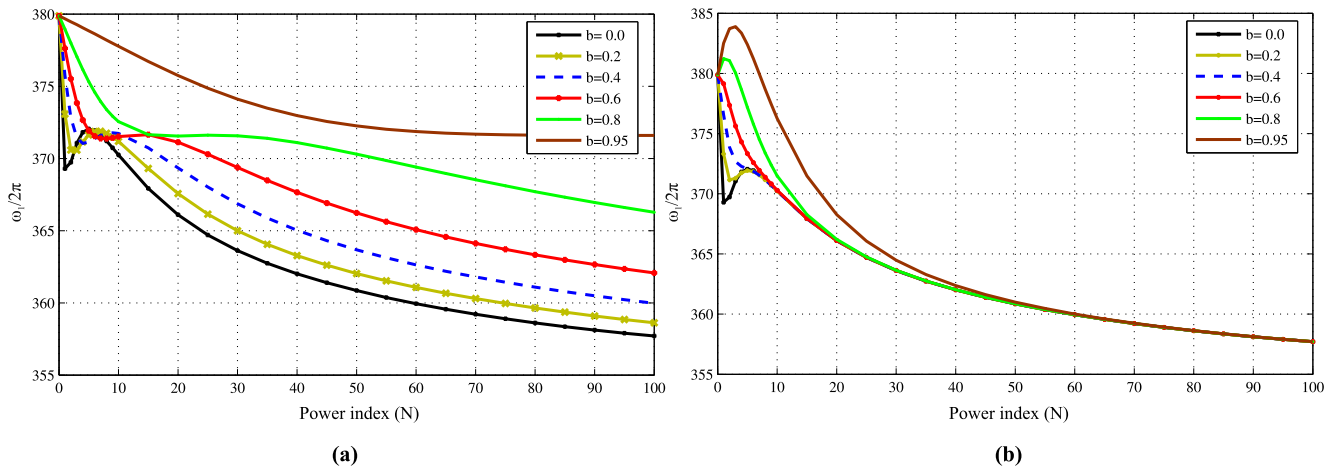
Fig. 20. Effects of the parameters b, c and N on the first natural frequencies of cracked a) $FGM_{(a=1/b/c=1/N)}$ b) $FGM_{(a=1/b/c=3/N)}$ spherical dome.

Acknowledgements

References

[1] Bushnell D. Stress, stability and vibration of complex, branched shells of revolution. Comput Struct 1974;4(2):399–424.

[2] Chung H. Free vibration analysis of circular cylindrical shells. J Sound Vib 1981;74(3):331–50.

[3] Lee Y-S et al. A study on the free vibration of the joined cylindrical–spherical shell structures. Comput Struct 2002;80(27):2405–14.

[4] Leissa AW, Vibration of plates; 1969. DTIC Document.

[5] Leissa AW. The free vibration of rectangular plates. J Sound Vib 1973;31 (3):257–93.

[6] Leissa AW. Vibration of shells. : Acoustical Society of America New York; 1993.

[7] Loy C, Lam K. Vibration of thick cylindrical shells on the basis of three-dimensional theory of elasticity. J Sound Vib 1999;226(4):719–37.

[8] Mustafa B, Ali R. An energy method for free vibration analysis of stiffened circular cylindrical shells. Comput Struct 1989;32(2):355–63.

[9] Loy C, Lam K, Reddy J. Vibration of functionally graded cylindrical shells. Int J Mech Sci 1999;41(3):309–24.

[10] Fazzolari FA. A refined dynamic stiffness element for free vibration analysis of cross-ply laminated composite cylindrical and spherical shallow shells. Compos B Eng 2014;62:143–58.

[11] Civalek Ö. Vibration analysis of laminated composite conical shells by the method of discrete singular convolution based on the shear deformation theory. Compos B Eng 2013;45(1):1001–9.

[12] Benachour A et al. A four variable refined plate theory for free vibrations of functionally graded plates with arbitrary gradient. Compos B Eng 2011;42 (6):1386–94.

[13] Neves A et al. A quasi-3D sinusoidal shear deformation theory for the static and free vibration analysis of functionally graded plates. Compos B Eng 2012;43(2):711–25.

[14] Pradyumna S, Bandyopadhyay J. Free vibration analysis of functionally graded curved panels using a higher-order finite element formulation. J Sound Vib 2008;318(1):176–92.

[15] Amabili M, Frosali G, Kwak M. Free vibrations of annular plates coupled with fluids. J Sound Vib 1996;191(5):825–46.

[16] Efraim E, Eisenberger M. Exact vibration analysis of variable thickness thick annular isotropic and FGM plates. J Sound Vib 2007;299(4):720–38.

[17] Nie G, Zhong Z. Vibration analysis of functionally graded annular sectorial plates with simply supported radial edges. Compos Struct 2008;84(2): 167–76.

[18] Wang H-J, Chen L-W. Vibration and damping analysis of a three-layered composite annular plate with a viscoelastic mid-layer. Compos Struct 2002;58 (4):563–70.

[19] Guan-Liang Q, Song-Nian G, Jie-Sheng J. A finite element model of cracked plates and application to vibration problems. Comput Struct 1991;39 (5):483–7.

[20] Huang C, Leissa A. Vibration analysis of rectangular plates with side cracks via the Ritz method. J Sound Vib 2009;323(3):974–88.

[21] Lee H, Lim S. Vibration of cracked rectangular plates including transverse shear deformation and rotary inertia. Comput Struct 1993;49(4):715–8.

[22] Liew K, Hung K, Lim M. A solution method for analysis of cracked plates under vibration. Eng Fract Mech 1994;48(3):393–404.

[23] Solecki R. Bending vibration of a simply supported rectangular plate with a crack parallel to one edge. Eng Fract Mech 1983;18(6):1111–8.

[24] Stahl B, Keer L. Vibration and stability of cracked rectangular plates. Int J Solids Struct 1972;8(1):69–91.

[25] Fantuzzi N, Tornabene F, Viola E. Four-parameter functionally graded cracked plates of arbitrary shape: a GDQFEM solution for free vibrations. Mech Adv Mater Struct 2016;23(1):89–107.

[26] Viola E, Tornabene F, Fantuzzi N. Generalized differential quadrature finite element method for cracked composite structures of arbitrary shape. Compos Struct 2013;106:815–34.

[27] Tornabene F et al. A numerical investigation on the natural frequencies of FGM sandwich shells with variable thickness by the local generalized differential quadrature method. Appl Sci 2017;7(2):131.

[28] Huang C, McGee O, Wang K. Three-dimensional vibrations of cracked rectangular parallelepipeds of functionally graded material. Int J Mech Sci 2013;70:1–25.

[29] Joshi P, Jain N, Ramtekkar G. Analytical modeling for vibration analysis of thin rectangular orthotropic/functionally graded plates with an internal crack. J Sound Vib 2015;344:377–98.

[30] Dolbow J, Belytschko T. A finite element method for crack growth without remeshing. Int J Numer Meth Eng 1999;46(1):131–50.

[31] Asadpoure A, Mohammadi S. Developing new enrichment functions for crack simulation in orthotropic media by the extended finite element method. Int J Numer Meth Eng 2007;69(10):2150–72.

[32] Asadpoure A, Mohammadi S, Vafai A. Crack analysis in orthotropic media using the extended finite element method. Thin-Walled Struct 2006;44(9):1031–8.

[33] Asadpoure A, Mohammadi S, Vafai A. Modeling crack in orthotropic media using a coupled finite element and partition of unity methods. Finite Elem Anal Des 2006;42(13):1165–75.

[34] Ashari S, Mohammadi S. Delamination analysis of composites by new orthotropic bimaterial extended finite element method. Int J Numer Meth Eng 2011;86(13):1507–43.

[35] Afshar A, Ardakani SH, Mohammadi S. Transient analysis of stationary interface cracks in orthotropic bi-materials using oscillatory crack tip enrichments. Compos Struct 2016;142:200–14.

[36] Motamedi D, Mohammadi S. Dynamic crack propagation analysis of orthotropic media by the extended finite element method. Int J Fract 2010;161(1):21–39.

[37] Motamedi D, Mohammadi S. Dynamic analysis of fixed cracks in composites by the extended finite element method. Eng Fract Mech 2010;77(17):3373–93.

[38] Nasirmanesh A, Mohammadi S. XFEM buckling analysis of cracked composite plates. Compos Struct 2015;131:333–43.

[39] Nasirmanesh A, Mohammadi S. Eigenvalue buckling analysis of cracked functionally graded cylindrical shells in the framework of the extended finite element method. Compos Struct 2017;159:548–66.

[40] Dimitri R et al. Numerical computation of the crack development and SIF in composite materials with XFEM and SFEM. Compos Struct 2017;160:468–90.

[41] Ardakani SH, Afshar A, Mohammadi S. Numerical study of thermo-mechanical coupling effects on crack tip fields of mixed-mode fracture in pseudoelastic shape memory alloys. Int J Solids Struct 2016;81:160–78.

[42] Ardakani SH, Ahmadian H, Mohammadi S. Thermo-mechanically coupled fracture analysis of shape memory alloys using the extended finite element method. Smart Mater Struct 2015;24(4):045031.

[43] Bayesteh H, Mohammadi S. XFEM fracture analysis of orthotropic functionally graded materials. Compos B Eng 2013;44(1):8–25.

[44] Goli E, Bayesteh H, Mohammadi S. Mixed mode fracture analysis of adiabatic cracks in homogeneous and non-homogeneous materials in the framework of partition of unity and the path-independent interaction integral. Eng Fract Mech 2014;131:100–27.

[45] Hosseini S, Bayesteh H, Mohammadi S. Thermo-mechanical XFEM crack propagation analysis of functionally graded materials. Mater Sci Eng, A 2013;561:285–302.

[46] Areias P, Rabczuk T. Finite strain fracture of plates and shells with configurational forces and edge rotations. Int J Numer Meth Eng 2013;94 (12):1099–122.

[47] Areias P, Rabczuk T, Msekh M. Phase-field analysis of finite-strain plates and shells including element subdivision. Comput Methods Appl Mech Eng 2016;312:322–50.

[48] Chau-Dinh T et al. Phantom-node method for shell models with arbitrary cracks. Comput Struct 2012;92:242–56.

[49] Nguyen-Thanh N et al. An extended isogeometric thin shell analysis based on Kirchhoff-Love theory. Comput Methods Appl Mech Eng 2015;284:265–91.

[50] Bhardwaj G et al. Numerical simulation of functionally graded cracked plates using NURBS based XIGA under different loads and boundary conditions. Compos Struct 2015;126:347–59.

[51] Natarajan S et al. Natural frequencies of cracked functionally graded material plates by the extended finite element method. Compos Struct 2011;93 (11):3082–92.

[52] Tran LV et al. Vibration analysis of cracked FGM plates using higher-order shear deformation theory and extended isogeometric approach. Int J Mech Sci 2015;96:65–78.

[53] Yin S et al. Buckling and vibration extended isogeometric analysis of imperfect graded Reissner-Mindlin plates with internal defects using NURBS and level sets. Comput Struct 2016;177:23–38.

[54] Bayesteh H, Mohammadi S. XFEM fracture analysis of shells: the effect of crack tip enrichments. Comput Mater Sci 2011;50(10):2793–813.

[55] Mohammadi S. Extended finite element method: for fracture analysis of structures. John Wiley & Sons; 2008.

[56] Natarajan S et al. A parametric study on the buckling of functionally graded material plates with internal discontinuities using the partition of unity method. Eur J Mech-A/Solids 2014;44:136–47.

[57] Natarajan S et al. Linear free flexural vibration of cracked functionally graded plates in thermal environment. Comput Struct 2011;89(15):1535–46.

[58] Huang C, McGee O, Chang M. Vibrations of cracked rectangular FGM thick plates. Compos Struct 2011;93(7):1747–64.

[59] Tornabene F. Free vibration analysis of functionally graded conical, cylindrical shell and annular plate structures with a four-parameter power-law distribution. Comput Methods Appl Mech Eng 2009;198(37):2911–35.

[60] Tornabene F, Viola E, Inman DJ. 2-D differential quadrature solution for vibration analysis of functionally graded conical, cylindrical shell and annular plate structures. J Sound Vib 2009;328(3):259–90.

[61] Qu Y et al. A unified formulation for vibration analysis of functionally graded shells of revolution with arbitrary boundary conditions. Compos B Eng 2013;50:381–402.

[62] Su Z, Jin G, Ye T. Three-dimensional vibration analysis of thick functionally graded conical, cylindrical shell and annular plate structures with arbitrary elastic restraints. Compos Struct 2014;118:432–47.